

# Adapting Vision-Language Foundation Model for Next Generation Medical Ultrasound Image Analysis

Jingguo Qu<sup>1</sup>, Xinyang Han<sup>1</sup>, Tonghuan Xiao<sup>1</sup>, Jia Ai<sup>4</sup>, Juan Wu<sup>4</sup>, Tong Zhao<sup>5</sup>,  
Jing Qin<sup>2</sup>, Ann Dorothy King<sup>3</sup>, Winnie Chiu-Wing Chu<sup>3</sup>, Jing Cai<sup>1</sup>, and  
Michael Tin-Cheung Ying<sup>1</sup>

<sup>1</sup> Department of Health Technology and Informatics, The Hong Kong Polytechnic University, Hong Kong, China

<sup>2</sup> Centre for Smart Health and School of Nursing, The Hong Kong Polytechnic University, Hong Kong, China

<sup>3</sup> Department of Imaging and Interventional Radiology, The Chinese University of Hong Kong, Hong Kong, China

<sup>4</sup> Suzhou Hospital of Traditional Chinese Medicine Affiliated to Nanjing University of Chinese Medicine, Suzhou, China

<sup>5</sup> Department of Ultrasound, The Affiliated Changzhou No. 2 People's Hospital of Nanjing Medical University, Changzhou, China

**Abstract.** Medical ultrasonography is an essential imaging technique for examining superficial organs and tissues, including lymph nodes, breast, and thyroid. It employs high-frequency ultrasound waves to generate detailed images of the internal structures of the human body. However, manually contouring regions of interest in these images is a labor-intensive task that demands expertise and often results in inconsistent interpretations among individuals. Vision-language foundation models, which have excelled in various computer vision applications, present new opportunities for enhancing ultrasound image analysis. Yet, their performance is hindered by the significant differences between natural and medical imaging domains. This research seeks to overcome these challenges by developing domain adaptation methods for vision-language foundation models. In this study, we explore the fine-tuning pipeline for vision-language foundation models by utilizing large language model as text refiner with special-designed adaptation strategies and task-driven heads. Our approach has been extensively evaluated on six ultrasound datasets and two tasks: segmentation and classification. The experimental results show that our method can effectively improve the performance of vision-language foundation models for ultrasound image analysis, and outperform the existing state-of-the-art vision-language and pure foundation models. The source code of this study is available at [GitHub](#).

**Keywords:** Foundation model · domain adaptation · fine-tuning · ultrasound · lymph node · breast lesion.

## 1 Introduction

Computed tomography (CT), magnetic resonance imaging (MRI) and ultrasonography (US) are common medical imaging modalities in clinical practice. Among these, US is particularly favored for evaluating superficial structures including breast lesions [5], thyroid nodules [31], and lymph nodes [37,2,1], because it offers real-time visualization with non-invasive and cost-effective characteristics. Utilizing high-frequency ultrasound, US delivers detailed views of internal anatomy and is routinely used in clinical examinations. Currently, radiologists need to manually identify and delineate regions of interest (ROIs) on ultrasound scans to diagnose diseases and develop treatment plans, which is a time-consuming process and subject to variability depending on the experiences of radiologists.

However, the natural imaging vulnerabilities of ultrasonography poses challenges to this process, including grainy appearance, ill-defined ROI boundaries, low contrast, and the introduction of artifacts. Furthermore, the shapes, sizes, and locations of ROIs can vary substantially across scan planes and patient anatomies. These factors make manual annotation laborious and inconsistent, underscoring the need for automated methods that can reliably detect, segment and classify ROIs to improve diagnostic efficiency and accuracy. Thus, automated ultrasound image analysis is a potential direction for standardized and regulated diagnosis and treatment.

Deep learning has driven significant advances in medical image analysis [11,10], but these methods rely on large volumes of expertly annotated data [30] and lack generalizability [27]. Foundation models [4], which are pre-trained on vast, diverse datasets offer a way to relax this requirement. By capturing broad visual representations during pre-training, they can be efficiently fine-tuned with few labeled ultrasound scans, while still maintaining coherent, task-relevant features. This paradigm holds great promise for more practical, data-efficient analysis in clinical practice. Yet, despite growing interest in adapting foundation models to specialized domains, their application to ultrasound image analysis remains under-explored.

Mainstream foundation models have shown impressive performance in various computer vision tasks, such as zero-shot classification [28], semantic segmentation [18,24] and visual-language interactions [32]. Although several studies [16,23] have investigated the application of foundation models in medical ultrasound image analysis, the efficacy of these specialized models, when trained solely on comparatively smaller ultrasound datasets, is still debated against the performance of original foundation models pre-trained on extensive natural image datasets [26]. Consequently, the development of domain adaptation techniques for specific downstream domains and tasks based on original foundation models remains a promising research direction.

To address this problem, this study proposes a simple and effective workflow for the foundation model domain adaptation from natural image distribution to ultrasound modality. Specifically, we optimized the pre-trained CLIP [28] in a parameter-efficient-fine-tuning manner by introducing a hierarchical adapter to the vision branch. To further enhance the visual representation capability for

ultrasound images with ROIs in various characteristics, and reduce the complexity of whole architecture, a straightforward up-sampling and adaptive pooling layer are integrated to the foundation model as head for specific downstream tasks. The proposed framework is evaluated on six ultrasound datasets: the in-house lymph node ultrasound datasets from two different centers (LN-1, LN-2), the public available breast ultrasound image (BUSI) dataset [3], thyroid datasets DDTI [25] and TN3K [9], and ultrasound scans of prostate [15]. The experimental findings demonstrate that the proposed framework surpasses existing methods including the original version of CLIP and other variants which were trained from scratch based on medical datasets.

## 2 Related Work

Foundation models (FMs) [4] represent a class of large-scale models pre-trained on vast datasets through self-supervised learning, enabling them to tackle a wide variety of tasks via transfer learning. Prominent examples include GPT [29], SAM [18], BERT [7], CLIP [28] and DINOv2 [24].

Among these, CLIP [28] distinguishes itself with a contrastive pre-training framework that aligns images and text within a shared embedding space by minimizing the cosine distance between correlated image-text pairs. This approach allows CLIP to perform zero-shot classification using text prompts such as "A photo of {class}" without additional re-training. In the medical domain, adaptations like PubMedCLIP [8] and MedCLIP [33] have primarily targeted visual question answering (VQA) tasks. Meanwhile, CLIPSeg [22] builds on this framework by incorporating support images alongside compact text prompts, extending its applicability to binary segmentation during inference time.

Numerous studies have investigated the applications of FMs in medical image analysis. Huix *et al.* [14] evaluated FMs on medical image classification tasks and found that, while these models can outperform state-of-the-art (SOTA) approaches pre-trained on ImageNet [6], their performance varies inconsistently across datasets of different scales, suggesting limitations in robustness and generalizability.

In contrast to leveraging original pre-trained weights, some researchers have pursued training CLIP-like models from scratch using exclusively medical data. PMC-CLIP [20] harnessed approximately one million biomedical image-text pairs from PubMed Central Open Access Subset across 12 modalities, achieving SOTA results in various downstream tasks such as image-text retrieval, image classification and medical VQA. BioMedCLIP [38] further scaled this effort by expanding the closed-source PMC-15M dataset to 15 million pairs. To address the gap of data transparency, UniMedCLIP [17] curated an open-source cross-modal dataset to pre-train a unified vision-language model, which comprising over 5.3 million samples and across six modalities.

Despite the evident importance of the scale of biomedical datasets demonstrated by these studies, the current sizes of curated datasets are significantly smaller than the original CLIP dataset, which consists of approximately 400

million natural image-text pairs. Research such as MetaCLIP [34] has established a clear positive correlation between the scale of datasets and model performance of CLIP and its variants. It is also been reinforced by Poudel *et al.* [26] that large-scale datasets offer advantages unattainable with smaller, domain-specific collections. Furthermore, most studies in this field primarily concentrated on sparse prediction tasks (*e.g.*, classification), while dense tasks (critical for detailed medical image analysis, *e.g.*, semantic segmentation) are still rarely reported.

Given the persistent challenge of obtaining large-scale, high-quality multi-modal medical datasets, domain adaptation of CLIP models pre-trained on expansive natural datasets emerges as a promising avenue for future research.

### 3 Method

The overall architecture of our method is illustrated in Fig. 1. Firstly, adapters such as low-rank adaptation (LoRA) [13] and multi-cognitive visual adapter (Mona) [36] are integrated into the visual branch of frozen CLIP. The curated and cleaned ultrasound image-caption pairs are utilized to facilitate CLIP fine-tuning. Secondly, segmentation and classification heads are attached to the image encoder merged with adapter to perform supervised tasks. Additionally, we create unified prompts for each disease represented in the ultrasound scans for CLIP zero-shot ability evaluation.

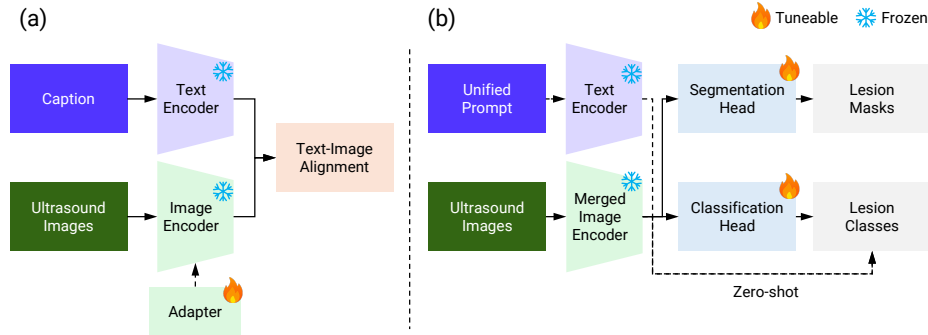


Fig. 1: Overview of proposed workflow. (a) **Fine-tuning stage.** Introduce trainable adapters into frozen CLIP to bridge the domain gap between natural images and ultrasound scans. (b) **Downstream tasks.** Apply trainable heads for ultrasound image segmentation and classification in a supervised manner (solid arrows), and assess zero-shot ultrasound diagnosis capability of CLIP by using unified prompt-image pairs (dashed arrows).

### 3.1 Fine-tuning

The present study places particular emphasis on two adapters, LoRA [13] and Mona [36], as illustrated in the Fig. 2.

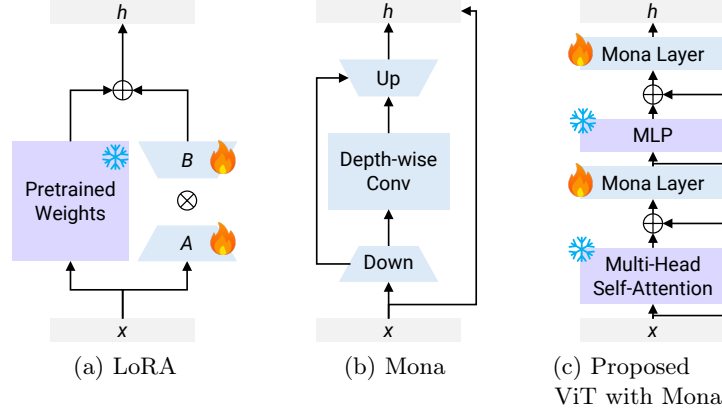


Fig. 2: Structure overview of the original LoRA, Mona and proposed ViT with Mona for CLIP visual backbone.

**LoRA.** To alleviate the computational burden of full fine-tuning, researchers introduced trainable low-rank matrices into specific layers, typically within the query, key, and value matrices in self-attention mechanism of Transformer. Instead of updating all model parameters, LoRA freezes the original weights and adapts the model via these additional low-rank matrices. This strategy significantly reduces the number of trainable parameters while still achieving performance comparable to fully fine-tuned models.

**Mona.** Unlike LoRA focuses on the specific components, Mona broadens its scope. First, the input is normalized, scaled, and down-sampled, and then three depth-wise convolutions ( $3 \times 3$ ,  $5 \times 5$ ,  $7 \times 7$ ) are applied to capture multi-scale visual patterns. The additional layer normalization and skip connections reshape and integrate features from the frozen backbone, resulting in more effective, task-specific visual representations.

Nonetheless, Mona was originally developed for Swin-Transformer [21] and cannot be directly applied to the standard Vision Transformer (ViT) used in visual backbone of CLIP. To overcome this, we embed Mona layers within a ViT architecture, as demonstrated in Fig. 2c. During fine-tuning, pre-trained weights of multi-head self-attention modules and the projection layer (multi-layer perceptron, MLP) remain frozen, while only the Mona layers are updated. This design allows for seamless integration with pre-trained CLIP weights when tackling downstream tasks.

### 3.2 Downstream Tasks

In this study, the downstream tasks comprise lesion segmentation and characteristics classification. To further reduce computational requirements while improving model performance and generalizability, we introduce several enhancements. The final segmentation and classification heads are shown in Fig. 3.

**Feature Reducing.** Inspired by CLIPSeg [22], we implement a mechanism that fuses select shallow and deep feature maps rather than aggregating representations from all 12 Transformer blocks of a standard ViT. Specifically, these sparsely chosen feature maps are projected to the same dimensionality as the vanilla CLIP feature space and then concatenated to form the input for the subsequent segmentation and classification heads.

**Feature Map Up-sampling.** Transformer feature maps typically exhibit low spatial resolution (*e.g.*,  $14 \times 14$  for a  $224 \times 224$  input with  $16 \times 16$  patch size). However, ROIs can vary significantly in size across different diseases and anatomical sites, making it challenging for CLIP to capture the fine-grained details required for dense prediction tasks. To address this, we integrate a bilinear up-sampling layer into both the segmentation and classification heads. This straightforward interpolation increases the resolution of feature maps and yields more detailed ROI representations and without introducing additional trainable parameters, in contrast to multi-layer transposed-convolutional designs.

**Adaptive Average Pooling.** In conventional architectures, classification heads often rely on MLPs. However, MLPs add a substantial number of trainable parameters and are prone to overfitting on limited datasets. In this work, we replace the MLP-based head with an adaptive average pooling layer, which introduces no trainable parameters. This design maintains computational efficiency and reduces overfitting risk while still delivering robust classification performance.

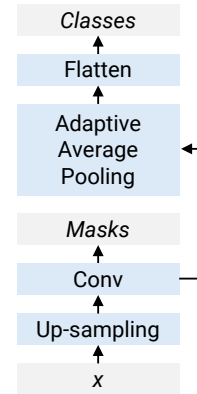


Fig. 3: Segmentation and classification heads.

## 4 Experiments

### 4.1 Datasets

There are three types of usage of datasets in this study, including fine-tuning (PMC-OA [20], CURD [19]), segmentation and classification. The overview of datasets and partitions are shown in Table 1.

**PMC-OA** [20] and **CURD** [19] serve as the primary data sources for fine-tuning process. The original PMC-OA dataset contains 1,848,719 images across various medical imaging modalities. From this collection, ultrasound images and their corresponding captions were extracted, while low-resolution images were excluded. The CURD dataset comprises ultrasound images and captions from 7,390 patients presenting with breast, liver, or thyroid abnormalities. Since

Table 1: Overview of datasets and partitions. Ft., Seg., and Cls. refer to fine-tuning, segmentation and classification tasks, respectively.

Dataset	Training	Validation	Testing	Total	Ft.	Seg.	Cls.
PMC-OA [20]	4,942	534	0	5,476	✓		
CURD [19]	13,228	1,500	0	14,728	✓		
LN-1	1,019	127	127	1,273		✓	✓
LN-2	0	0	374	374		✓	✓
BUSI [3]	518	65	64	647		✓	✓
DDTI [25]	510	64	63	637		✓	
TN3K [9]	2,304	575	614	3,493		✓	
Prostate [15]	1,937	215	758	2,910		✓	

the captions in CURD are in Chinese, we employ the Qwen3-8B [35] model to translate them into English and simultaneously refine the captions to conform to the 77-token limit required by CLIP models.

**Lymph Node (LN).** We collected two LN datasets, LN-1 comprises 1,273 ultrasound images of 307 cases, with years ranging from 2016 to 2024, and LN-2 includes of 374 images. All images are annotated at the pixel level by experienced radiologists to delineate the LN region. Notably, LN-2 is used exclusively as an external test set and is not involved in any part of the training process.

**BUSI [3].** There are 780 breast lesion ultrasound images in BUSI, with 437 benign, 210 malignant and 133 normal cases. The normal cases without ROIs are excluded in the following experiments as the purpose of this study is to detect and segment the abnormal regions.

**DDTI [25].** The DDTI dataset consists of 637 ultrasound images of thyroid nodules. The dataset includes a wide range of lesion types including focal thyroiditis, cystic nodules, adenomas and thyroid cancer.

**TN3K [9].** The TN3K dataset was collected at Zhujiang Hospital, Southern Medical University. For each patient, only one representative image is retained from those captured at similar viewpoints or anatomical locations. The dataset comprises 2,879 images for training and 614 images for testing.

**Prostate [15].** This dataset comprises both expert and non-expert prostate annotations of 75 patients, and only the expert annotations are used in this study.

## 4.2 Settings

**Implementation Details.** Prior to training, to minimize the impact of irrelevant information, non-imaging regions containing overlay annotations are cropped from all ultrasound images. Subsequently, all images are resized to  $224 \times 224$  pixels for both training and testing. An overview of the datasets and their partitions is provided in Table 1. Except for TN3K [9] and Prostate [15], all datasets are randomly divided into training, validation, and test sets in an 8:1:1 ratio. For

TN3K and Prostate, the predefined training set is further split into training and validation subsets using an 8:2 ratio, while the original test set remains unchanged.

The default learning rate for both fine-tuning and downstream tasks was set to  $10^{-4}$ , using a cosine annealing scheduler and a weight decay of  $10^{-2}$ . The loss functions used are cross-entropy loss for fine-tuning, Dice cross-entropy loss for segmentation, and focal loss for classification. All experiments utilize the AdamW optimizer with  $\beta_1 = 0.9$  and  $\beta_2 = 0.95$ , and the batch size is set to 32. All experiments were conducted on a single Nvidia RTX 4090 GPU with 24 GB memory.

**Evaluation Metrics.** We used four widely-used metrics to evaluate the segmentation performance of the proposed method: Dice score (Dice, %), intersection over union (IoU, %), 95 percentile of Hausdorff distance (HD95, %), and average symmetric surface distance (ASD, %). For classification, accuracy (Acc, %) and area under receiver operating characteristic curve (AUC, %) are adopted as evaluation metrics. All metrics are calculated based on the binary segmentation and classification results and averaged across all images in the test set.

### 4.3 Perquisites

The SOTA CLIP variants used for comparison in this study include BioMedCLIP [38], UniMedCLIP [17], and MetaCLIP [34]. To establish a visual-only performance baseline, we also evaluate models that rely solely on image input, including UNet [30], ResNet18 [12], and DINOv2 [24]. For all experiments and comparisons, we adopt the ViT-Base architecture with a patch size of  $16 \times 16$  pixels as the standard backbone. Pre-trained weights are used when publicly available for the respective models.

Given that zero-shot classification inference process of CLIP necessitates text information as a form of guidance, the subsequent prompts for ultrasound image classification task are devised. Instead of directly adopting the vanilla rough prompt and ,following the fixed format, we opt to utilize detailed descriptions of benign and malignant lesions as prompts. These prompts are intentionally limited to a maximum length of 77 tokens to prevent them from being truncated before input to text encoder.

1. **LN:** "Benign: Oval shape, preserved echogenic hilum, thin homogeneous cortex. Malignant: Round, absent hilum, thickened/heterogeneous cortex, microcalcifications, irregular margins.The abnormality in this lymph node scan is {benign/malignant}".
2. **BUSI:** "Benign: Oval shape, smooth margins, parallel orientation, homogeneous hypoechoic echotexture, posterior enhancement. Malignant: Irregular shape, spiculated margins, non-parallel orientation, heterogeneous hypoechoic echotexture, microcalcifications, posterior acoustic shadowing. The abnormality in this breast scan is {benign/malignant}".



To ensure the validity of the comparisons, the proposed head which incorporates feature map up-sampling and adaptive average pooling for downstream tasks, was employed for all CLIP variants. It is important to note that LN-2 is exclusively employed for evaluation purposes; consequently, the test results for LN-2 are derived directly from the model that was trained using LN-1.

#### 4.4 Segmentation Results

The quantitative segmentation results are shown in Table 2. It is evident that the proposed method CLIP (Mona) without fine-tuning exhibits optimal performance across all datasets. This leading trend reached its maximum in the LN-1, LN-2, and TN3K datasets, where our proposed method outperforms the second-best method CLIPSeg [22] by 4.91%, 4.53%, and 4.76% in Dice score, respectively.

Table 2: Segmentation experiment results based on six ultrasound datasets. All results are averaged with three runs and in percentage. The results of UNet are used for reference and not involved in comparisons. The ↓ indicates the smaller value the better, and ft. in braces refers to fine-tuned CLIP. The **best** and second best results are highlighted in bold and underline, respectively.

Method	LN-1				LN-2				BUSI			
	Dice	IoU	HD95↓	ASD↓	Dice	IoU	HD95↓	ASD↓	Dice	IoU	HD95↓	ASD↓
UNet	79.72	71.67	20.18	7.35	75.68	65.40	33.34	11.56	82.19	72.88	23.83	8.05
CLIP (LoRA)	73.37	62.84	23.63	8.12	73.96	62.93	27.24	9.18	78.86	68.64	19.46	6.53
CLIP (LoRA, ft.)	74.10	63.55	23.56	8.29	73.50	62.08	28.73	9.73	78.55	68.39	20.56	6.79
CLIPSeg	<b>78.21</b>	<b>68.98</b>	<b>21.21</b>	<b>7.91</b>	<b>74.38</b>	<b>64.30</b>	<b>25.97</b>	<b>8.76</b>	<b>80.74</b>	<b>71.32</b>	<b>16.69</b>	<b>5.77</b>
BioMedCLIP	72.62	63.00	28.81	9.19	67.63	55.95	33.05	11.25	77.07	65.92	27.08	8.79
UniMedCLIP	74.59	64.50	30.13	10.66	70.74	58.99	35.80	12.13	76.44	65.61	28.98	9.74
MetaCLIP	70.69	59.36	28.19	10.24	69.45	57.28	35.58	11.39	75.63	63.82	33.64	10.80
DINOv2	63.02	50.29	111.22	43.23	20.54	12.61	332.36	208.71	64.31	52.05	117.25	48.80
CLIP (Mona)	<b>83.12</b>	<b>75.41</b>	<b>16.71</b>	<b>5.70</b>	<b>78.91</b>	<b>68.79</b>	<b>23.58</b>	<b>7.77</b>	<b>80.78</b>	<b>70.90</b>	<b>19.07</b>	<b>6.27</b>
CLIP (Mona, ft.)	70.97	61.09	25.76	10.53	59.20	47.98	39.13	15.27	67.02	55.37	32.92	12.59
Method	DDTI				TN3K				Prostate			
	Dice	IoU	HD95↓	ASD↓	Dice	IoU	HD95↓	ASD↓	Dice	IoU	HD95↓	ASD↓
UNet	88.96	80.58	19.01	6.74	81.55	72.83	21.20	6.92	92.73	88.50	12.45	3.82
CLIP (LoRA)	88.22	79.34	18.40	7.16	76.38	65.61	29.02	9.38	90.43	84.60	18.10	5.71
CLIP (LoRA, ft.)	87.92	78.86	18.81	7.18	76.60	65.86	27.36	8.83	90.69	85.08	17.44	5.40
CLIPSeg	<b>89.18</b>	<b>80.86</b>	<b>17.29</b>	<b>6.39</b>	<b>77.91</b>	<b>67.80</b>	<b>21.58</b>	<b>7.25</b>	<b>91.32</b>	<b>86.26</b>	<b>13.30</b>	<b>4.27</b>
BioMedCLIP	88.17	79.29	19.59	7.22	73.40	62.06	32.43	10.63	91.20	85.30	19.66	6.01
UniMedCLIP	88.84	80.27	17.76	6.80	72.68	61.49	33.63	11.56	90.43	84.61	18.62	5.93
MetaCLIP	87.72	78.51	20.64	7.75	72.42	60.76	39.13	13.17	90.25	83.83	30.12	8.75
DINOv2	85.98	75.94	52.54	20.90	60.76	47.64	119.25	45.79	86.92	79.10	82.77	27.28
CLIP (Mona)	<b>90.26</b>	<b>82.61</b>	<b>15.75</b>	<b>5.91</b>	<b>82.67</b>	<b>73.58</b>	<b>17.85</b>	<b>5.68</b>	<b>92.58</b>	<b>88.15</b>	<b>11.17</b>	<b>3.76</b>
CLIP (Mona, ft.)	85.76	75.70	19.91	8.38	69.25	57.94	28.46	10.74	90.38	84.62	13.93	4.81

Across all six datasets, CLIP (Mona) exceeds in Dice and IoU scores of all competitors and the HD95 and ASD metrics are noticeably lower than others, indicating highly precise boundary delineation. These findings indicate that CLIP (Mona) can learn robust, transferable ultrasound representations on small ultrasound datasets. Notably, when CLIP (Mona) was subsequently fine-tuned on

limited data (CLIP (Mona, ft.)), its performance deteriorated across all datasets. This decline likely stems from catastrophic forgetting, wherein small-scale fine-tuning disrupts the generalized ultrasound features acquired during extensive pre-training. Consequently, fine-tuning CLIP with scarce annotated data may be counterproductive.

This observation also can be found when CLIP (LoRA) was further fine-tuned on limited ultrasound data (CLIP (LoRA, ft.)), no substantial improvement or slightly regression was detected. This suggests that small-scale fine-tuning may induce over-fitting or perturb the pre-trained feature representations without yielding meaningful gains.

Three medical CLIP variants were evaluated, including BioMedCLIP [38], UniMedCLIP [17], and MetaCLIP [34]. All of them have been trained from scratch on large-scale radiological or multi-modal medical datasets. Contrary to expectations, none of these domain-specific models surpasses CLIPSeg [22] or matches CLIP (Mona) performance. We attribute these weaknesses to the modality gap: although these models are trained on CT, MRI, *etc.*, and associated clinical text, their representations may cannot generalize directly to the heterogeneous acoustic signatures of ultrasound, and their pre-training objectives were not explicitly aligned with downstream dense prediction tasks.

We randomly selected one sample per test set of the six datasets for visualization and is shown in Fig. 4. A thorough examination reveals that the proposed method CLIP (Mona) exhibits superior performance in comparison to all other methods across all datasets, especially when applied to the TN3K [9] dataset. These visual results demonstrate a consistent pattern with prior quantitative analysis results.

Furthermore, the visual results also indicate that the CLIP variants (BioMedCLIP [38], UniMedCLIP [17]) which were trained on medical image-text dataset from scratch may not have the capacity for ultrasound image segmentation, compares to the vanilla CLIP [28] and CLIPSeg [22].

This phenomenon may be attributed to two factors. First, the scale of the medical dataset is considerably smaller than that of the natural dataset of vanilla CLIP (15 million pairs for BioMedCLIP, 5.3 million pairs for UniMedCLIP, versus 400 million pairs for CLIP). This discrepancy results in inadequate development of the model. Second, the corresponding texts for natural images within the CLIP dataset demonstrate a relatively simple and fixed pattern, such as "A photo of {class}". Nevertheless, the corpus of medical texts is mainly composed of diagnostic reports, which are considerably complex than general descriptions and characterized by high information density. This characteristic of medical texts presents a significant challenge to the model to learn the correlation between images and text.

Moreover, as demonstrated in Table 2 and Fig. 4, the DINOv2 [24] exhibited the poorest performance across all datasets. Although the dataset of DINOv2 contains 142 million images and is equivalent to the number of images of CLIP, DINOv2 lacks dense support information from text during the self-supervised contrastive learning procedure. Due to this reason and the considerable domain

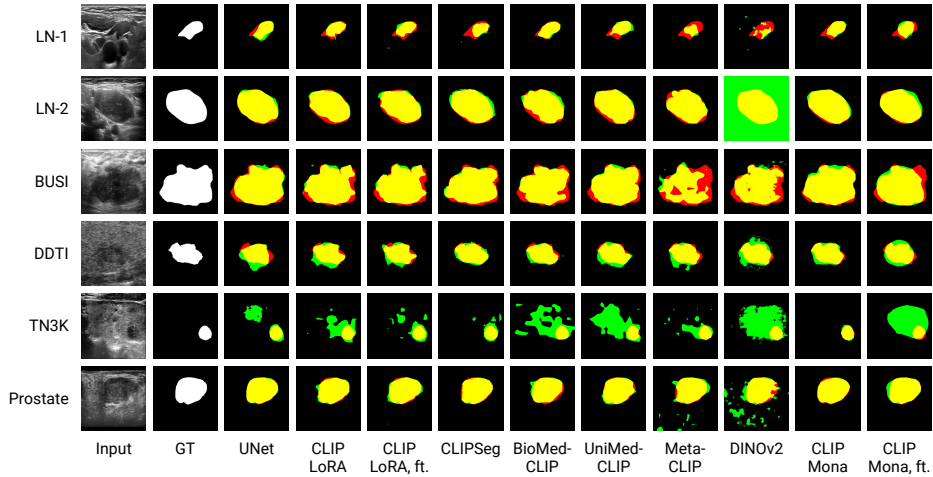


Fig. 4: Visualization of the proposed method and SOTAs on LN-1, LN-2, BUSI [3], DDTI [25], TN3K [9], and Prostate [15] datasets. The first and second columns show the original images and ground truth masks, respectively. Regions in red, green and yellow indicate the ground truth, false positive and true positive, respectively.

gap between pre-training images and ultrasound images, all pixels in the input image have been predicted as false positives for the LN-2 case. Concurrently, DINOv2 produces notable uncertainties for other scenarios (*i.e.*, scattered green areas), ultimately results in downgraded performance.

#### 4.5 Classification Results

In this study, we evaluated a range of CLIP-based models and adaptation strategies on three ultrasound classification datasets (LN-1, LN-2, and BUSI [3]) as only they were labeled with diagnostic classes (*i.e.*, benign and malignant) according to the confirmed pathology results. The quantitative results for the binary classification are illustrated in Table 3.

Across all datasets, zero-shot results of vanilla CLIP and variants of CLIP [28] with adapters demonstrated classification accuracies exhibit a high degree of consistency and only marginally above random guessing, with AUC scores hovering near 50%. These results make clear that, without any supervised fine-tuning on domain-specific ultrasound images, the pre-trained representations of CLIP are insufficient to support clinically meaningful classification.

CLIP (LoRA, ft.) yields mixed but promising results and has made a notable improvement compares to the version that without fine-tuning process, gaining up to 3.64% increase across three datasets. These results suggest that LoRA adaptation combined with supervised fine-tuning can harness the pre-trained features of CLIP to approach SOTA performance. This is particularly evident

Table 3: Classification experiment results based on six ultrasound datasets. All results are averaged with three runs and in percentage. The results of ResNet18 are used for reference and not involved in comparisons. The ft. in braces refers to fine-tuned CLIP. The **best** and second best results are highlighted in bold and underline, respectively.

Group	Method	LN-1		LN-2		BUSI	
		Acc	AUC	Acc	AUC	Acc	AUC
Zero-shot	CLIP (vanilla)	58.13	52.30	61.76	64.69	57.50	50.73
	CLIP (LoRA)	58.13	52.30	61.76	64.69	57.50	50.73
	CLIP (LoRA, ft.)	58.44	52.40	61.50	64.66	57.34	50.67
	CLIP (Mona)	58.13	52.30	61.76	64.69	57.50	50.73
	CLIP (Mona, ft.)	58.13	52.30	61.76	64.69	57.50	50.73
Supervised	ResNet18	85.30	93.59	73.26	84.16	88.24	94.61
	CLIP (LoRA)	82.68	91.88	67.38	78.14	83.34	91.60
	CLIP (LoRA, ft.)	85.04	<b>93.60</b>	70.86	83.40	<b>86.98</b>	<u>91.63</u>
	BioMedCLIP	<u>85.57</u>	92.89	70.86	81.04	83.86	90.80
	UniMedCLIP	83.99	91.29	<u>72.10</u>	<u>84.54</u>	82.81	<b>95.63</b>
	MetaCLIP	<b>88.19</b>	<u>93.59</u>	66.84	81.13	<u>84.38</u>	88.23
	DINOv2	79.53	84.34	49.20	62.92	37.50	65.62
	CLIP (Mona)	82.68	92.03	69.79	80.34	83.33	87.57
	CLIP (Mona, ft.)	80.31	85.87	<b>73.80</b>	<b>85.04</b>	77.60	82.64

on datasets with more homogeneous lesion characteristics, while it may struggle when sample diversity is higher or data scarcity is more pronounced (as in LN-2).

Among the domain-specific CLIP variants, performance varied considerably. BioMedCLIP [38] achieved a second best accuracy on LN-1 while MetaCLIP [34] demonstrated the maximum, but its performance on other datasets was both unstable and generally inferior to other CLIP variants. UniMedCLIP [17] exhibited the highest AUC on BUSI [3]. These observations indicate that medical CLIPs cannot consistently outperform baseline across all tasks. Data imbalance in pre-training modalities (*e.g.*, CT/X-ray vs. ultrasound) and differences in supervised objectives may account for the observed variability in transferability.

Further supervised fine-tuning of CLIP (Mona, ft.) led to a substantial performance boost on LN-2 (73.80% accuracy and 85.04% AUC), surpassing all competitors. However, the fine-tuned version shows a significant performance degradation compared with the vanilla CLIP with Mona on the other two datasets. This pattern suggests that small-scale fine-tuning can induce catastrophic forgetting, and further efforts are necessary to enhance the generalizability and consistency of fine-tuning processes.

Finally, DINOv2 [24] shows poor performance across all three datasets. These results imply that, in the absence of ultrasound-specific supervision or adaptation, the DINOv2 fail to discriminate the malignancy for either LNs or the breast lesions effectively.

## 4.6 Key Findings

1. It has been demonstrated that, irrespective of the presence or absence of fine-tuning via ultrasound image-text datasets, vanilla CLIP [28] and CLIP variants are incapable of ultrasound image diagnosis capabilities in the zero-shot manner.
2. General medical CLIP (BioMedCLIP [38], UniMedCLIP [17], MetaCLIP [34]) exhibit unstable transfer ability to ultrasound, often yielding lower Dice and higher boundary errors, which suggests a requirement for ultrasound-tailored pre-training objectives.
3. CLIP variants achieve optimal segmentation performance but suffer from catastrophic forgetting when fine-tuned on small labeled sets, highlighting the need for robust fine-tuning strategies.

## 5 Conclusion

In this study, we comprehensively validate the capability of the vision-language foundation model (CLIP) for ultrasound image analysis. We investigate the impact of fine-tuning CLIP on ultrasound image-text datasets and conduct a thorough performance comparison among the vanilla CLIP, CLIP variants augmented with domain-adaptation components, and other CLIP models pre-trained on pure medical image-text pairs. We also propose semantic segmentation and classification heads that combine feature-map up-sampling with adaptive average pooling, which significantly improve performance while reducing the number of trainable parameters. The experimental results on six ultrasound datasets demonstrate that the domain-adapted CLIP model for ultrasound achieves superior results in comparison to those of all competitors in the semantic segmentation task. Subsequent efforts should prioritize the enhancement of the classification performance of domain-adapted CLIP models.

**Acknowledgments.** This work was supported by General Research Funds of the Research Grant Council of Hong Kong (Reference no. 15102222 and 15102524).

**Disclosure of Interests.** The authors have no competing interests to declare that are relevant to the content of this article.

## References

1. Ahuja, A.T., Ying, M., Ho, S.Y., Antonio, G., Lee, Y.P., King, A.D., Wong, K.T.: Ultrasound of malignant cervical lymph nodes. *Cancer Imaging* **8**(1), 48–56 (2008). <https://doi.org/10.1102/1470-7330.2008.0006>
2. Ahuja, A.T., Ying, M.: Sonographic evaluation of cervical lymph nodes. *American Journal of Roentgenology* **184**(5), 1691–1699 (2005). <https://doi.org/10.2214/ajr.184.5.01841691>
3. Al-Dhabyani, W., Gomaa, M., Khaled, H., Fahmy, A.: Dataset of breast ultrasound images. *Data in Brief* **28**, 104863 (2020). <https://doi.org/10.1016/j.dib.2019.104863>

4. Bommasani, R., Hudson, D.A., Adeli, E., Altman, R., Arora, S., von Arx, S., Bernstein, M.S., Bohg, J., Bosselut, A., Brunskill, E., et al.: On the opportunities and risks of foundation models. arXiv:2108.07258 (2021)
5. Brem, R.F., Lenihan, M.J., Lieberman, J., Torrente, J.: Screening breast ultrasound: Past, present, and future. *American Journal of Roentgenology* **204**(2), 234–240 (2015). <https://doi.org/10.2214/AJR.13.12072>
6. Deng, J., Dong, W., Socher, R., Li, L.J., Li, K., Fei-Fei, L.: Imagenet: A large-scale hierarchical image database. In: 2009 IEEE conference on computer vision and pattern recognition. pp. 248–255. Ieee (2009)
7. Devlin, J., Chang, M.W., Lee, K., Toutanova, K.: Bert: Pre-training of deep bidirectional transformers for language understanding. In: North American Chapter of the Association for Computational Linguistics (2019)
8. Eslami, S., de Melo, G., Meinel, C.: Does clip benefit visual question answering in the medical domain as much as it does in the general domain? ArXiv **abs/2112.13906** (2021)
9. Gong, H., Chen, J., Chen, G., Li, H., Li, G., Chen, F.: Thyroid region prior guided attention for ultrasound segmentation of thyroid nodules. *Computers in Biology and Medicine* **155**, 106389 (2023). <https://doi.org/10.1016/j.compbiomed.2022.106389>
10. Han, M.X., Ying, M.T.C., Qu, M.J., Chen, Z., Gunda, M.S.T., Cai, J., Qin, J., Chu, W.C.W., King, A.D.: Differentiation of benign and malignant lymph nodes using ultrasound-based radiomics and machine learning. *Journal of Medical Imaging and Radiation Sciences* **55**(3), 101544 (2024)
11. Han, X., Qu, J., Chui, M.L., Gunda, S.T., Chen, Z., Qin, J., King, A.D., Chu, W.C.W., Cai, J., Ying, M.T.C.: Artificial intelligence performance in ultrasound-based lymph node diagnosis: a systematic review and meta-analysis. *BMC cancer* **25**(1), 73 (2025)
12. He, K., Zhang, X., Ren, S., Sun, J.: Deep residual learning for image recognition. In: Proceedings of the IEEE conference on computer vision and pattern recognition. pp. 770–778 (2016)
13. Hu, E.J., Shen, Y., Wallis, P., Allen-Zhu, Z., Li, Y., Wang, S., Wang, L., Chen, W., et al.: Lora: Low-rank adaptation of large language models. *ICLR* **1**(2), 3 (2022)
14. Huix, J.P., Ganeshan, A.R., Haslum, J.F., Söderberg, M., Matsoukas, C., Smith, K.: Are natural domain foundation models useful for medical image classification? In: Proceedings of the IEEE/CVF winter conference on applications of computer vision. pp. 7634–7643 (2024)
15. Jiang, H., Imran, M., Muralidharan, P., Patel, A., Pensa, J., Liang, M., Benidir, T., Grajo, J.R., Joseph, J.P., Terry, R.S., DiBianco, J.M., Su, L., Zhou, Y., Brisbane, W., Shao, W.: Microsegnet: A deep learning approach for prostate segmentation on micro-ultrasound images. *Computerized medical imaging and graphics : the official journal of the Computerized Medical Imaging Society* **112**, 102326 (2023)
16. Jiao, J., Zhou, J., Li, X., Xia, M., Huang, Y., Huang, L., Wang, N., Zhang, X., Zhou, S., Wang, Y., et al.: Usfm: A universal ultrasound foundation model generalized to tasks and organs towards label efficient image analysis. *Medical Image Analysis* **96**, 103202 (2024)
17. Khattak, M.U., Kunhimon, S., Naseer, M., Khan, S., Khan, F.S.: Unimed-clip: Towards a unified image-text pretraining paradigm for diverse medical imaging modalities. arXiv preprint arXiv:2412.10372 (2024)
18. Kirillov, A., Mintun, E., Ravi, N., Mao, H., Rolland, C., Gustafson, L., Xiao, T., Whitehead, S., Berg, A.C., Lo, W.Y., Dollár, P., Girshick, R.: Segment anything. arXiv:2304.02643 (2023)

19. Li, J., Su, T., Zhao, B., Lv, F., Wang, Q., Navab, N., Hu, Y., Jiang, Z.: Ultrasound report generation with cross-modality feature alignment via unsupervised guidance. *IEEE Transactions on Medical Imaging* (2024)
20. Lin, W., Zhao, Z., Zhang, X., Wu, C., Zhang, Y., Wang, Y., Xie, W.: Pmc-clip: Contrastive language-image pre-training using biomedical documents. In: *International Conference on Medical Image Computing and Computer-Assisted Intervention*. pp. 525–536. Springer (2023)
21. Liu, Z., Lin, Y., Cao, Y., Hu, H., Wei, Y., Zhang, Z., Lin, S., Guo, B.: Swin transformer: Hierarchical vision transformer using shifted windows. In: *Proceedings of the IEEE/CVF international conference on computer vision*. pp. 10012–10022 (2021)
22. Lüddecke, T., Ecker, A.: Image segmentation using text and image prompts. In: *Proceedings of the IEEE/CVF conference on computer vision and pattern recognition*. pp. 7086–7096 (2022)
23. Meyer, A., Murali, A., Mutter, D., Padoy, N.: Ultrasam: A foundation model for ultrasound using large open-access segmentation datasets. *arXiv:2411.16222* (2024)
24. Oquab, M., Darcet, T., Moutakanni, T., Vo, H., Szafraniec, M., Khalidov, V., Fernandez, P., Haziza, D., Massa, F., El-Nouby, A., et al.: Dinov2: Learning robust visual features without supervision. *arXiv:2304.07193* (2023)
25. Pedraza, L., Vargas, C., Narváez, F., Durán, O., Muñoz, E., Romero, E.: An open access thyroid ultrasound image database, Tenth International Symposium on Medical Information Processing and Analysis, vol. 9287. SPIE (2015). <https://doi.org/10.1117/12.2073532>
26. Poudel, K., Dhakal, M., Bhandari, P., Adhikari, R., Thapaliya, S., Khanal, B.: Exploring transfer learning in medical image segmentation using vision-language models. In: *International Conference on Medical Imaging with Deep Learning* (2023)
27. Qu, J., Han, X., Chui, M.L., Pu, Y., Gunda, S.T., Chen, Z., Qin, J., King, A.D., Chu, W.C.W., Cai, J., Ying, M.T.C.: The application of deep learning for lymph node segmentation: A systematic review. *IEEE Access* **13**, 97208–97227 (2025). <https://doi.org/10.1109/ACCESS.2025.3575454>
28. Radford, A., Kim, J.W., Hallacy, C., Ramesh, A., Goh, G., Agarwal, S., Sastry, G., Askell, A., Mishkin, P., Clark, J., et al.: Learning transferable visual models from natural language supervision. In: *International conference on machine learning*. pp. 8748–8763. PmLR (2021)
29. Radford, A., Narasimhan, K., Salimans, T., Sutskever, I., et al.: Improving language understanding by generative pre-training (2018)
30. Ronneberger, O., Fischer, P., Brox, T.: U-net: Convolutional networks for biomedical image segmentation. In: *Medical image computing and computer-assisted intervention—MICCAI 2015: 18th international conference, Munich, Germany, October 5–9, 2015, proceedings, part III 18*. pp. 234–241. Springer (2015)
31. Takashima, S., Fukuda, H., Nomura, N., Kishimoto, H., Kim, T., Kobayashi, T.: Thyroid nodules: Re-evaluation with ultrasound. *Journal of Clinical Ultrasound* **23**(3), 179–184 (1995). <https://doi.org/10.1002/jcu.1870230306>
32. Wang, J., Chen, D., Wu, Z., Luo, C., Zhou, L., Zhao, Y., Xie, Y., Liu, C., Jiang, Y.G., Yuan, L.: Omnivl: One foundation model for image-language and video-language tasks. *Advances in neural information processing systems* **35**, 5696–5710 (2022)
33. Wang, Z., Wu, Z., Agarwal, D., Sun, J.: Medclip: Contrastive learning from unpaired medical images and text. *Proceedings of the Conference on Empirical Methods in Natural Language Processing*. *Conference on Empirical Methods in Natural Language Processing* **2022**, 3876–3887 (2022)

34. Xu, H., Xie, S., Tan, X.E., Huang, P.Y., Howes, R., Sharma, V., Li, S.W., Ghosh, G., Zettlemoyer, L., Feichtenhofer, C.: Demystifying clip data. arXiv preprint arXiv:2309.16671 (2023)
35. Yang, A., Li, A., Yang, B., Zhang, B., Hui, B., Zheng, B., Yu, B., Gao, C., Huang, C., Lv, C., et al.: Qwen3 technical report. arXiv preprint arXiv:2505.09388 (2025)
36. Yin, D., Hu, L., Li, B., Zhang, Y., Yang, X.: 5% > 100%: Breaking performance shackles of full fine-tuning on visual recognition tasks. arXiv preprint arXiv:2408.08345 (2024)
37. Ying, M., Ahuja, A.: Sonography of neck lymph nodes. part i: Normal lymph nodes. *Clinical Radiology* **58**(5), 351–358 (2003). [https://doi.org/10.1016/S0009-9260\(02\)00584-6](https://doi.org/10.1016/S0009-9260(02)00584-6)
38. Zhang, S., Xu, Y., Usuyama, N., Xu, H., Bagga, J., Tinn, R., Preston, S., Rao, R., Wei, M., Valluri, N., et al.: Biomedclip: a multimodal biomedical foundation model pretrained from fifteen million scientific image-text pairs. arXiv preprint arXiv:2303.00915 (2023)